Invited paper

OPTO-ELECTRONICS REVIEW **8**(2), 91–100 (2000)

Simulation of optical phenomena in vertical-cavity surface-emitting lasers II. Models

W. NAKWASKI*

Institute of Physics, Technical University of Łódź
219 Wólczańska Str., 93-005 Łódź, Poland
and
Centre for High Technology Materials, University of New Mexico
Albuquerque, NM 87106, 1313 Goddard SE, USA

Various theoretical approaches used to model optical fields inside resonators of vertical-cavity surface-emitting lasers (VCSELs) are described in the present paper. Both simplified and advanced simulations developed for both index-guided and gain-guided VCSELs are presented. Reviews of both scalar (mostly for standard VCSEL designs polarised not very far over their thresholds) and vectorial (for microresonator VCSELs as well as in more exact modelling of standard VCSELs) optical VCSEL models known from scientific literature are also given.

Keywords: vertical-cavity surface-emitting lasers (VCSELs), optical models, simulation approaches, Maxwell equations.

1. Introduction

Comprehensive computer simulations of a diode laser describe its operation with the aid of many mutually interrelated mathematical equations formulated for individual physical processes taking place within a laser cavity during a device operation. They are supplemented by expressions giving values of device and material parameters dependent on local conditions, i.e. material compositions, temperature, carrier concentrations, an electric field, a radiation intensity, etc. Such simulations may be used to examine more deeply physical phenomena and interactions between individual physical processes taking place within the laser volume during its operation. Therefore advanced simulation approaches enable us to understand better physics of these devices in its whole complexity. This knowledge may be used to modify laser designs and even to optimise them for specified applications.

Fundamental principles of modelling optical phenomena in vertical-cavity surface-emitting lasers (VCSELs) are given in the first part of this paper [1]. In particular, electric ($\vec{E}$) and magnetic ($\vec{H}$) field vectors of the laser radiation have been found to obey the following vector wave equation

$$(\nabla^2 + k_0^2 N_R^2)\vec{\psi} = 0, \tag{1}$$

where ∇ is the Nabla operator (∇^2 is the vector Laplacian), k_0 stands for the wave number, $\vec{\psi}$ may be either $\vec{E}$ or $\vec{H}$ vectors, and N_R is the complex index of refraction

$$N_R = n_R - ik_e, \tag{2}$$

with n_R standing for the refractive index and k_e for the extinction coefficient. $\vec{E}$ or $\vec{H}$ profiles are critical in determination of many important interactions in diode lasers, in particular – the interaction between carrier distributions and a laser optical field, which is an essence of a laser operation itself. Therefore knowledge of the above profiles are crucial to simulate any semiconductor laser.

The above one vector wave equation (1) may be reduced to the following six scalar wave equations

$$(\Delta + k_0^2 N_R^2)\Phi_i = 0, \tag{3}$$

for each Φ_i (i = x, y, z or i = r, z, φ) component of the $\vec{E}$ and $\vec{H}$ vectors. In the above relation, Δ stands for the scalar Laplacian.

Depending on structure details, various approaches have been used to optical modelling of VCSELs. In this second part of the paper, optical models developed for various VCSEL designs will be presented. The paper is organised as follows. The solution of the scalar wave equation in the VCSEL configuration is presented in Section 2. Sections 3 and 4 are devoted to simplified scalar approaches to the index-guided (IG) VCSELs and the gain-guided (GG) VCSELs, respectively. Sections 5 and 6 present review of scalar and vectorial VCSEL optical models, respectively, known from scientific literature, which are followed by conclusions.

*e-mail: nakwaski@ck-sg.p.lodz.pl

2. Solution of the scalar wave equation

On the basis of our considerations presented in the first part [1] of the paper, in standard VCSEL designs of rather wide active regions, it is justified to assume that the emitted radiation is linearly polarised in the plane parallel to the active-region plane (and perpendicular to the propagation direction). So for this very often case, we may reduce our considerations to one scalar wave equation of the form given by Eq. (3) rather than to the more complicated vector one (1). Also, because of cylindrical symmetry of most of VCSEL devices, from now on we are using (unless indicated differently) the cylindrical (r,z,φ) co-ordinate system (see Fig. 3 in Ref. 1), with z directed along the symmetry axis, r perpendicular to it and φ is the azimuthal angle.

For the VCSEL laser light linearly polarised in the plane perpendicular to the direction of propagation (assumed to be along the z-axis)

$$\Phi_T^{k,m,s}(r,z,\varphi) = \exp(i\omega_{k,m,s}t)\exp(i\beta_s z)\Phi_T^{k,m}(r,\varphi), \quad (4)$$

where Φ_T is any transverse component of $\vec{E}$ or $\vec{H}$ vectors and k, m, and s are the orders of azimuthal, transverse and longitudinal modes of the laser radiation, respectively, the scalar wave equation (3) is reduced to

$$\frac{1}{r}\frac{\partial}{\partial r}\left(r\frac{\partial \Phi_T^{k,m}(r,\varphi)}{\partial r}\right) + \frac{1}{r^2}\frac{\partial^2 \Phi_T^{k,m}(r,\varphi)}{\partial \varphi^2} + [k_0^2 N_R^2 - \beta_s^2] = 0. \quad (5)$$

Taking into consideration cylindrical VCSEL symmetry, the solution of the above equation may be assumed in a following simple form [2,3]:

$$\Phi_T^{k,m}(r,\varphi) = R_{km}(r)\exp(ik\varphi), \quad (6)$$

which transforms Eq. (5) to

$$\frac{d^2R_{km}(r)}{dr^2} + \frac{1}{r}\frac{dR_{km}(r)}{dr} + \left(k_0^2 N_R^2 - \beta_s^2 - \frac{k^2}{r^2}\right)R_{km}(r) = 0 \quad (7)$$

For k = 0, the solution of the above equation is a mixture of the fundamental HE_{11} mode (the LP_{01} mode) and the HE_{1m} (m>1) modes (the LP_{0m} modes). For the higher k, also the TE_{0m}, the TM_{0m}, and the $HE_{(k+1)m}$ modes (i.e. the LP_{km} modes) can be found. Usually only one longitudinal s^{th} mode (if any) may be excited in VCSELs [4], but still several azimuthal k^{th} and transverse m^{th} modes may be present in their emission.

3. The simplified approach to IG VCSELs

In the case of weakly index-guided (IG) VCSELs, the homogeneous refractive index in the central part of the resonator (n_{R1}) is somewhat higher than that of surrounding areas (n_{R2}) assumed to extend to infinity, i.e., for $(n_{R1}-n_{R2})/n_{R1} << 1$ and $n_{R1} > n_{R2}$

$$n_{RA}(r) = \begin{cases} n_{R1} & for\ |r| \le r_A \\ n_{R2} & for\ |r| \ge r_A \end{cases}, \quad (8)$$

where r_A is the radius of the active region. Then, for the case of a negligible gain-guiding effect and for a laser light linearly polarised in a plane perpendicular to the direction of propagation, assumed to be along the z axis, transverse field component E_T (for transverse H_T component the equation is analogous) in the k^{th} azimuthal mode, the m^{th} transverse mode and the s^{th} longitudinal mode may be written in the well known, classical form [5]:

$$E_T^{k,m,s} = E_{k,m,s}\exp(ik\varphi)\exp(i\beta_s z)\times \begin{cases} J_k(ur/r_A)/J_k(u) & for\ |r| \le r_A \\ K_k(vr/r_A)/K_k(v) & for\ |r| \ge r_A \end{cases}, \quad (9)$$

where $E_{k,m,s}$ is the electric field at the interface $r = r_A$, β_s stands for the propagation constant for the s^{th} longitudinal mode, which should be determined from boundary conditions, and J_k and K_k are the Bessel functions and the modified Hankel functions, respectively, both of the k^{th} order. The complex u and v parameters may be determined from the following relations:

$$u = r_A(k_0^2 n_{R1}^2 - \beta_s^2)^{1/2}, \quad (10)$$

$$v = r_A(\beta_s^2 - k_0^2 n_{R2}^2)^{1/2}. \quad (11)$$

The above simple approach is sometimes mistakenly applied to more often used GG VCSELs, where its assumptions are undoubtedly not justified.

Resulting above solutions are called the LP_{km} modes, which in fact are usually sets of modes, for example $LP_{01} = HE_{11}$, $LP_{11} = HE_{21} + TM_{01} + TE_{01}$, $LP_{02} = HE_{12}$, $LP_{12} = HE_{22} + TM_{02} + TE_{02}$, $LP_{03} = HE_{13}$, $LP_{13} = HE_{23} + TM_{03} + TE_{03}$, $LP_{04} = HE_{14}$, etc. When optical fields do not depend on the φ-coordinate (k = 0), single mode fields can be obtained. In a uniform layer, one can always find pure TE_{0m} and TM_{0m} modes. Otherwise all modes in cylindrically symmetric dielectric waveguides are hybrid modes, containing both electric and magnetic components [6] and not vanishing E_z and H_z components.

Let us introduce a unit polarisation vector $\vec{1}_p$. Then the vector optical field $\vec{\psi}$ may be expressed as follows

$$\vec{\psi}(r,z,\varphi) = \vec{1}_p\,\psi(r,z,\varphi). \quad (12)$$

It is also convenient to normalise the optical field (r,z,φ)

$$\frac{1}{\pi r_A^2 d_A}\int_0^L\int_0^{r_A}\int_0^{2\pi}|\psi(r,z,\varphi)|^2 r\,dr\,d\varphi\,dz = 1, \quad (13)$$

where d_A is the active region thickness, L is the resonator length, and r_s is the structure radius. Analogously, also all $\Phi_i(r,z,\varphi)$ fields are assumed to be normalised.

4. The simplified approach to GG VCSELs

The comprehensive thermal-electrical self-consistent simulation [7] of an operation of typical GG VCSELs, i.e. the proton-implanted top-surface-emitting lasers (PITSELs), has revealed that the temperature and carrier-concentration radial profiles within the broad central part of their active regions have parabolic shapes. Therefore PITSEL resonators may be approximately treated as the complex square law (CSL) media. The above means that effective values of both the index of refraction (n_R) and the optical gain g (which is directly proportional to the exctinction coefficient k_e), i.e., of both the real and imaginary parts of the complex effective index of refraction N_R [c.f. Eq. (2)], are varying in the active-region plane inside PITSEL resonators approximately parabolically:

$$n_R(r) = n_{R,0} - a_n r^2, \tag{14}$$

$$g(r) = g_0 + a_g r^2, \tag{15}$$

where r is the radial coordinate, whereas $n_{R,0}$, g_0, a_n, and a_g are constants. It was found [8] that in the CSL medium the transverse modes may be expressed analytically in a form of the Hermite-Gaussian functions as

$$\psi_{pq}(x,y,z) = \frac{\sqrt{2/\pi}}{\sqrt{2^{p+q}\,p!\,q!\,w}} H_p\left(\sqrt{2}\,\frac{x}{w}\right) H_q\left(\sqrt{2}\,\frac{y}{w}\right) \times \exp\left[-\left(\frac{k_0}{2}\right)(a+ib)\,r^2\right] \exp(-i\beta_{pq} z), \tag{16}$$

where p and q are the mode orders in the x and y directions, respectively, k_0 stands for the wave vector in vacuum, $r^2 = x^2 + y^2$, H_p and H_q are the Hermite polynomials [9], β_{pq} is the longitudinal propagation constant [8]:

$$\beta_{pq} = k_0\left(n_{R,0} + i\frac{\lambda}{4\pi} g_0\right) - \frac{p+q+1}{n_{R,0}}(a+ib), \tag{17}$$

and

$$a^2 = \sqrt{a_n^2 n_{R,0}^2 + a_g^2 n_{R,0}^2 / 4k_0^2} + a_n n_{R,0}, \tag{18}$$

$$b^2 = \sqrt{a_n^2 n_{R,0}^2 + a_g^2 n_{R,0}^2 / 4k_0^2} - a_n n_{R,0}, \tag{19}$$

w is the halfwidth of the laser beam

$$w^{-2} = \frac{k_0}{2}(a+ib). \tag{20}$$

In the above Eq. (17), λ is the radiation wavelength.

The Hermite polynomials H_p and H_q [9] may be written using the Rodrigues' formulae as [8,10]:

$$H_{p(q)}(x) = (-1)^{p(q)} \exp(x^2) \frac{d^{p(q)}}{dx^{p(q)}} \exp(-x^2), \tag{21}$$

or in an explicit expressions as [9]:

$$H_n(x) = n! \sum_{m=0}^{N} \frac{(2x)^{n-2m}}{m!(n-2m)!}, \tag{22}$$

where N is the largest integer equal to or less than n/2. For the lowest n arguments the above relation is reduced to the following forms

$$H_0(x) = 1, \tag{23a}$$

$$H_1(x) = 2x, \tag{23b}$$

$$H_2(x) = 4x^2 - 2, \tag{23c}$$

$$H_3(x) = 8x^3 - 12x, \tag{23d}$$

$$H_4(x) = 16x^4 - 48x^2 + 12. \tag{23e}$$

Near-field intensity profiles [11] are shown in Fig. 1 for the lowest-order transverse modes of a typical PITSEL. The fundamental 00 mode is symmetrically situated in the central part of the resonator, as expected. The 10 mode has two side-maxima penetrating partly the lossy $r > r_A = 5$ μm area. This penetration is even more intense in the case of the 20 mode, for which intensity maxima nearly coincide with the active-region edge. Surprisingly, the central maximum of this mode is not seen as for the analogous mode obtained for the step-like distributions of the refractive index (see Section 3). In fact, this maximum exists, which is confirmed by Fig. 2, but because of complex interactions [12] between various guiding and antiguiding effects, it is suppressed, and practically disappears. Similar behaviour is observed for other higher-order transverse modes exhibiting seemingly less numbers of intensity maxima than expected. Hence the number of such maxima on experimental near-field VCSEL profiles cannot be used to indicate the mode order, as it is often thought.

5. Review of scalar optical VCSEL models

In standard VCSELs of rather wide active regions, it is justified to assume that their radiation is linearly polarised in the plane parallel to the active-region plane at least just over their thresholds (c.f. Section 3 of Ref. 1). Therefore in this often case, one scalar wave equation (3) may be used instead of more complicated its vectorial form (1). Until now many scalar optical models of VCSEL operation have been reported. In this section, some of them will be presented.

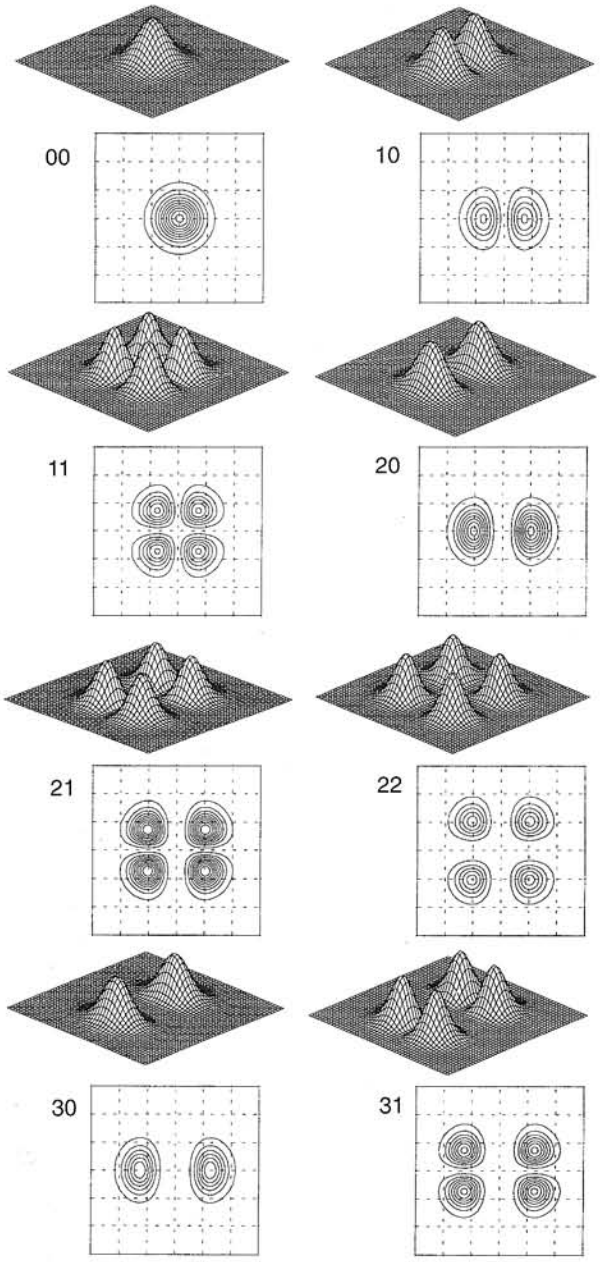

Fig. 1. Near-field intensity profiles of the lowest-order (00,10,11,20,21,22,30, and 31) transverse modes of the typical PITSEL with the active-region radius $r_A = 5$ μm and supplied with the current 6 mA.

In 1995 Zhang and Petermann [13] adopted the beam-propagation (BP) method to analysing optical-field propagation in VCSELs. Applicability of this method is restricted to relatively simple VCSEL designs. Besides, only an averaged (with respect to the azimuthal angle) radial profile of an optical field in a VCSEL resonator is typically obtained with this method, although it is possible to separate it into even and odd modes [14]. Nevertheless Zhang and Petermann used this method and considered the optical field in a VCSEL resonator as a superposition of a forward travelling wave Φ_α^+ and a backward travelling wave Φ_α^- in the active (α = a) and the spacer (α = s) sections

$$\Phi_i(r,z) = \Phi_{i\alpha}^+(r,z)\exp(-ik_{i\alpha}z) + \Phi_{i\alpha}^-(r,z)\exp(ik_{i\alpha}z)\,, \qquad (24)$$

where $k_{i\alpha}$ is the wave number in the α^{th} section $k_{i\alpha} = 2\pi n_{R\alpha}/\lambda$ with $n_{R\alpha}$ being its refractive index. Substituting Eq. (24) to Eq. (3) and neglecting the higher-order terms we reach two paraxial equations for the forward (+) and the backward (–) waves travelling between resonator mirrors:

$$\pm\frac{\partial\Phi_{i\alpha}^{\pm}(r,z)}{\partial z} = \frac{i}{2k_{i\alpha}}\left[\frac{1}{r}\frac{\partial}{\partial r}\left(r\frac{\partial}{\partial r}\right) + \Delta\varepsilon_\alpha(r)k_0^2\right]\Phi_{i\alpha}^{\pm}(r,z)\,, \qquad (25)$$

where

$$\Delta\varepsilon_\alpha = n_{R\alpha}\left(i\frac{\alpha - g}{k_0} + 2\frac{\partial n_{R\alpha}}{\partial T}\Delta T + 2\frac{\partial n_{R\alpha}}{\partial n}\Delta n\right), \qquad (26)$$

with α (loss), g (gain), ΔT (temperature increase), and Δn (carrier-concentration increase) being local values of indicated quantities. Equation (25) enables recalculation of the optical-field profile step by step during its propagation.

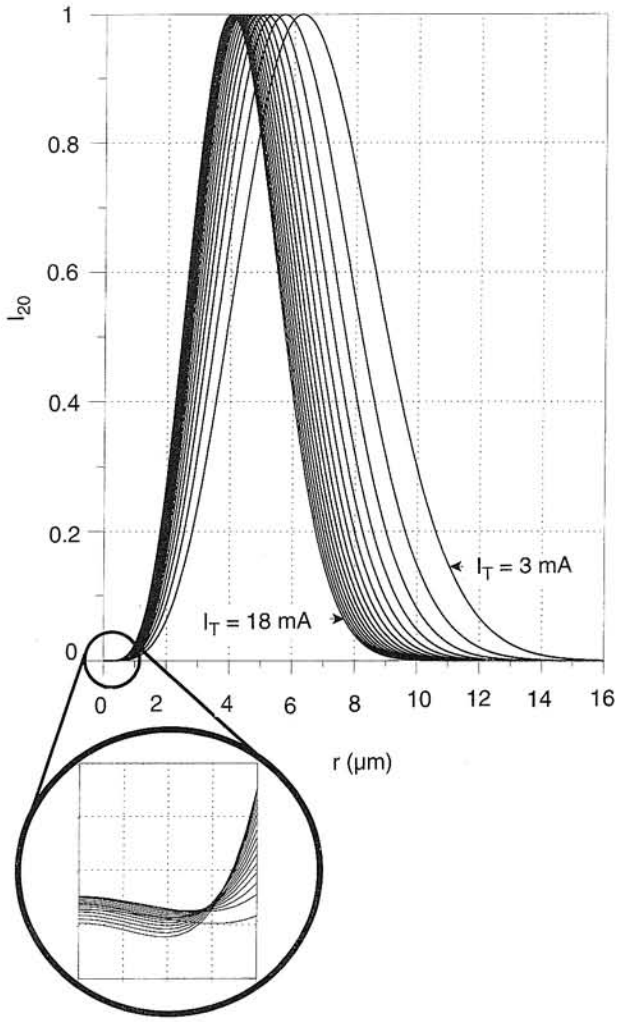

Fig. 2. Radial intensity profiles (in arbitrary units) determined for the 20 mode of the 5-μm PITSEL for operation currents changing by 1 mA from 3 to 18 mA. Their central parts were magnified to show central maxima.

The above BP approach has been successfully applied by Wilk *et al.* [15] to investigate the radial spatial hole-burning (SHB) effect in PITSELs their comprehensive self-consistent electro-opto-thermal simulation. The model has contained detailed thermal and electrical parts, therefore also self-focusing and thermal-waveguiding effects as well as many other interactions between physical phenomena have been included [16]. For a typical 5.5-μm PITSEL, three-dimensional views of intensity profiles in the active-region plane obtained using this approach are shown in Fig. 3 for two values of an operating current. The profiles turned out to be distinctly of a doughnut shape with a broad minimum around the centre of the active region and a ring-form maximum close to its perimeter. Similar intensity profiles were obtained experimentally by Wilson *et al.* [17] and were attributed just to the radial SHB effect.

Yu and Lo [18] have been also using the BP approach to model IG VCSELs introducing, however, the SHB effect as the only interaction between electrical and optical phenomena. This approach has been somewhat modified by Yu *et al.* [19] and Yu [20,21], but its considerable improvement has been just reported very recently by Man and Yu [22]. In their simulation of the proton-implanted bottom-emitting GG VCSEL, they have taken into account not only the SHB effect, but also the self-focusing effect and the temperature dependencies of laser threshold currents and the voltage drop at the p-n junction. Surprisingly, although the model has contained an ample thermal part, many temperature related phenomena have been neglected,

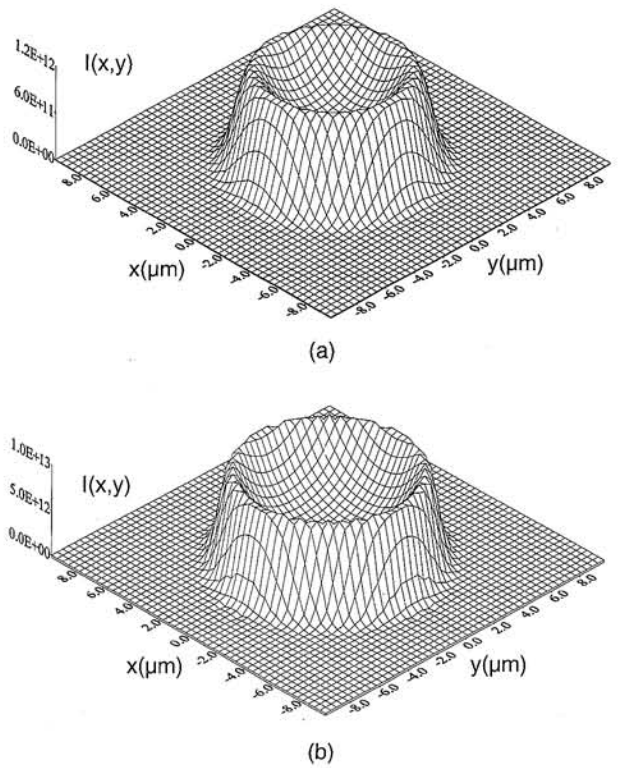

Fig. 3. Intensity profiles in the active-region plane determined for the 5.5-μm PITSEL supplied with the operation current 3 mA (a) and 18 mA (b)

including the thermal-waveguiding effect and temperature influences on both electrical resistivities and thermal conductivities of constituent semiconductor layers as well as on gain parameters and absorption coefficients. This approach has been recently modified by Yu [23], but the above shortcomings have not been removed.

In scalar approaching to optical properties of the edge-emitting lasers (EELs), the effective-index method was successfully applied. Its applicability for VCSELs has been also proposed by Hadley [24]. The method implies approximate separability of the optical field $\Phi(r,z,\varphi)$

$$\Phi(r,z,\varphi) \approx Z(z)\Phi_T(r,\varphi)\,. \tag{27}$$

Then the wave equation is separated into its longitudinal and transverse parts and structure details decided about its optical properties are embodied in the so-called effective index.

Hadley *et al.* [25] have applied the effective-index method to comprehensive simulation of an operation of both the PITSEL GG VCSEL and the oxide-confined IG VCSEL. In the simulation, many interactions between individual physical processes have been included in a self-consistent manner, e.g., the SHB effect, the thermal-waveguiding effect, and the temperature-dependent current leakage. Surprisingly, many other interactions have been neglected, including the self-focusing effect as well as temperature dependencies of thermal conductivities (in an explicit form) and of electrical resistivities of semiconductor layers, and also of the local gain, optical losses, and recombination coefficients. Nevertheless, the model is very sophisticated, and at the moment of its publishing, it was probably the most comprehensive VCSEL simulation.

In 1997 Wenzel and Wünsche [26] proposed the most advanced scalar approach to optical phenomena in VCSELs known until now. Principally, the method is a modified version of the effective-index method, obtained by an additional incorporation of the temporal dispersion of the dielectric constant. Hence the averaged frequency rather is containing information about structure details than the average index of refraction, the authors called this method: the effective-frequency method. Using the expansion around a real reference angular frequency ω_R

$$k_0^2 N_R^2 = \frac{\omega^2}{c^2} N_R^2 \approx \frac{\omega_R^2}{c^2} N_R^2 + 2\frac{\omega_R}{c^2} N_R N_G (\omega - \omega_R)\,, \tag{28}$$

where N_G is the complex group index defined as $N_G = \partial(\omega N_R)/\partial\omega$, we may transform the scalar wave equation (3) into

$$[\Delta + k_R^2 N_R^2(r,z,\varphi)]\Phi_i(r,z,\varphi) = \\ = \nu k_R^2 N_R(r,z,\varphi) N_G(r,z,\varphi)\Phi_i(r,z,\varphi), \tag{29}$$

where $k_R = \omega_R/c$ and the dimensionless frequency parameter ν defined as

$$\nu \equiv 2\frac{\omega_R - \omega}{\omega_R} = 2\frac{\lambda - \lambda_R}{\lambda} - i\frac{2\,\mathrm{Im}(\omega)}{\omega_R}, \qquad (30)$$

plays now a role of the eigenvalue. As in the case of the effective-index method, the effective-frequency method is associated with separability of the $\Phi_i(r,z,\varphi)$ function into two approximately one-dimensional functions

$$\Phi_i(r,z,\varphi) = f(r,z,\varphi)\Phi_T(r,\varphi), \qquad (31)$$

where the f function is assumed to be normalised and to fulfil the following longitudinal wave equation

$$\left[\frac{\partial^2}{\partial z^2} + k_R^2 N_R^2(r,z,\varphi)\right] f(r,z,\varphi) = \\ = \nu_{eff}(r,\varphi)\, k_R^2 N_R(r,z,\varphi) N_G(r,z,\varphi) f(r,z,\varphi), \qquad (32)$$

at each lateral position (r,φ). So the structure is divided into a number of cylindrically symmetric sectors. For each of them, constant and uniform distributions of refractive indices as well as loss or gain coefficients within all individual layers are assumed (but they may be different in different layers and different in different sectors). For each such a sector, the longitudinal wave Eq. (32) is solved. Principally, the f(z) functions and the effective frequencies ν_{eff} may be different at every position (r,φ). Assuming, however, cylindrical symmetry of a device, we may obtain one effective frequency ν_{eff} and one f(z) function for each region, which means – for each r value. Then we may write the transverse wave equation in the following form

$$\left[\frac{1}{r}\frac{d}{dr}\left(r\frac{d}{dr}\right) - \frac{k^2}{r^2} + \nu_{eff}(r)\, k_R^2 \langle N_R N_G \rangle_r\right] R_{km}(r) = \\ = \nu_{km} k_R^2 \langle N_R N_G \rangle_r R_{km}(r). \qquad (33)$$

The radial field distribution is determined with the aid of the transverse wave equation (33) for the complex index of refraction in a structure averaged in the z-direction, as if the waveguide were nearly uniform, although slow radial changes of losses (or gain) and the refractive index are also included. For each k^{th} azimuthal mode, each solution of the transverse wave equation (33) composes different m^{th} mode with a different value of the frequency parameter ν_{km} (an eigenvalue). The algorithm needs some self-consistency, because the effective frequency ν_{eff} is present in both the nearly one-dimensional wave equations (32) and (33). Solutions of the above equation are again LP_{km} modes. The effective-frequency method enables easy determination of the threshold condition for each (k,m) mode, requiring: $\mathrm{Im}(\nu_{km})_{th} = 0$.

The effective-frequency method has been recently applied to analyse complex optical structures of nitride-based intracavity-contacted VCSELs [27]. This optical model has been coupled with the comprehensive thermal-electrical VCSEL simulation [28,29]. Calculated gain profile exhibits distinctly nonuniform distribution with a sharp maximum close to the active-region edge and a deep minimum in the centre. Not surprisingly, such a gain profile has strong impact on mode profiles. Poor overlap between the gain profile and the fundamental LP_{01} mode results in its strong suppression, which is followed by the LP_{21} mode becoming the most favoured one.

6. Review of vectorial optical VCSEL models

Scalar approaches to optical fields in VCSELs require solving only one wave equation for an assumed linearly polarised light. Fully vectorial approaches, on the other hand, need considering six equations (12) for all (r,z,φ) or (x,y,z) components of both fields $\vec{E}$ and $\vec{H}$. Therefore, vectorial simulations of optical VCSEL properties are not only more complex but they also require more computer memory and more CPU time to be implemented.

The first vectorial analysis of optical fields in VCSELs was reported by Thode *et al.* [30] in 1994 as a part of their time-dependent comprehensive VCSEL simulation. They were solving the Maxwell equations using the finite-difference (FD) algorithm, which, if carried out for the whole laser volume, would require extensive mainframe computer resources to be implemented. Therefore, to shorten necessary CPU time, the simulation region was somewhat arbitrarily limited to only a cylinder of 12-μm radius and 6.75-μm height. A uniform mesh was used in both longitudinal and radial directions within the cylinder, therefore 80 uniform regions of average material parameters were defined. In thermal and electrical parts of the model, transport equations of six independent variables were solved: the electric potential, the electron and hole densities, the electron and hole temperatures, and the lattice temperature. In the model, many mechanisms of energy exchange were taken into consideration, including the Auger recombination and the impact ionisation as well as the Shockley-Read-Hall recombination and the phonon scattering.

The above approach seems to be premature at the moment of its creation and even now, similarly as next simulations of this kind reported by Ning *et al.* [31–34]. New achievements of such an approach (e.g. different temperatures assumed for electrons, holes and phonons) are too subtle to have practical meaning now. Besides, there are also some essential drawbacks of this analysis. First of all, it considers important laser variables (e.g. temperature, carrier concentrations, and current densities) as position independent, average quantities, whereas their 3D profiles are often very nonuniform and these nonuniformities are very important in accurate modelling of a VCSEL operation. Furthermore, most of decay rates in the kinetic equations are used as adjustable parameters. All construction and material details essential for a proper VCSEL operation are hidden in these parameters. Finally, the above parameters depend, for example, on VCSEL thermal and electrical resistances, whose exact determination now seems to be

more essential for modelling VCSEL operation than a subtle distinction between temperatures of lattice and plasma. The distinction should be included, however, into modern VCSEL models in future, when new computers enable us to extend the present 3D models without the above mentioned limitations.

Fully vectorial study of optical VCSEL properties was reported in 1996 by Demeulenaere *et al.* [35]. They considered an idealised VCSEL structure composed of optically uniform layers. Then, in each structure layer and for each i^{th} radiation mode, its propagation may be expressed as

$$\vec{\Psi}_i(r,z,\varphi,t) = \vec{\Psi}_i(r,\varphi)\exp(i\beta_s z)\exp(-i\omega t). \quad (34)$$

Assuming an ideally cylindrical structure symmetry, z-components of the fields within this layer may be written as

$$E_z^i(r,\varphi) = E_z^i(r)\cos(k\varphi), \quad (35)$$

$$H_z^i(r,\varphi) = H_z^i(r)\sin(k\varphi). \quad (36)$$

Then these components may be found from the following equations

$$\left[\frac{1}{r}\frac{d}{dr}\left(r\frac{d}{dr}\right)+k_0^2 n_R^2 - \beta_s^2 - \frac{k^2}{r^2}\right]\begin{pmatrix} E_z^i(r) \\ H_z^i(r)\end{pmatrix} = 0, \quad (37)$$

and all other field components are related to z-components in a following way [36]:

$$E_\varphi^i(r,\varphi) = \frac{i\sin(k\varphi)}{k_0^2 n_R^2 - \beta_s^2}\left[-\frac{k\beta_s}{r}E_z^i(r) - \omega\mu_0\frac{dH_z^i(r)}{dr}\right], \quad (38)$$

$$E_r^i(r,\varphi) = \frac{i\cos(k\varphi)}{k_0^2 n_R^2 - \beta_s^2}\left[\beta_s\frac{dE_z^i(r)}{dr} + \frac{k\omega\mu_0}{r}H_z^i(r)\right], \quad (39)$$

$$H_\varphi^i(r,\varphi) = \frac{i\cos(k\varphi)}{k_0^2 n_R^2 - \beta_s^2}\left[\frac{k\beta_s}{r}H_z^i(r) + \omega n_R^2\varepsilon_0\frac{dE_z^i(r)}{dr}\right], \quad (40)$$

$$H_r^i(r,\varphi) = \frac{i\sin(k\varphi)}{k_0^2 n_R^2 - \beta_s^2}\left[\frac{\beta_s}{r}\frac{dH_z^i(r)}{dr} + \frac{k\omega n_R^2\varepsilon_0}{r}E_z^i(r)\right], \quad (41)$$

where a discrete set of β_s values corresponds to successive s^{th} longitudinal modes and should be found from the boundary conditions. From Eq. (37), the z-components may be found in a following form

$$\begin{pmatrix} E_z^i(r) \\ H_z^i(r)\end{pmatrix} = \begin{pmatrix} A_E \\ A_H\end{pmatrix} J_k(u_i r), \quad (42)$$

where A_E and A_H are modes amplitudes and u_i may be expressed as

$$u_i^2 = k_0^2 n_R^2 - \beta_s^2. \quad (43)$$

In this idealised VCSEL structure of optically uniform layers, the optical field may be composed of pure TE and TM modes. But, because a distribution of a complex index of refraction in such layers is strongly influenced by nonuniform profiles of temperature and carrier concentrations, each real VCSEL layer is optically nonuniform, even if it has been manufactured from a material of an exactly the same and uniform composition. Demeulenaere *et al.* [35] were looking for the electromagnetic field in each separate optically-nonuniform layer in a form of a series using above presented solutions to the Maxwell equations in the same, but uniform this time, layer as vectorial basis functions [37,38], which makes finding optical-field profiles using this method an extremely time-consuming task.

Burak and Binder [39,40] reported in 1997 a similar approach, in which optical fields in a real VCSEL structure were expanded into so called cold-cavity modes, obtained first for a simplified case of a structure without gain and losses. For all six components of $\vec{E}$ and $\vec{H}$ vectors, solutions of the Maxwell equations were found in an analytical form for this simplified case. As in the above approach of Demeulenaere *et al.* [35], the total optical field is a superposition of the TE and the TM modes and has a form of hybrid HE modes. For a real VCSEL structure with gain and losses, transverse components of both the electric and magnetic fields in each k^{th} layer were expressed as a superposition in a complete set of orthogonal cold-cavity hybrid modes found in the previous step of the calculations. In this simulation, a vectorial transform matrix approach has been used. The method is very exact, but it also involves intense numerical calculations. Some electro-optical interactions have been included in Ref. 41.

In their similar vectorial approach to modelling an optical field in the VCSEL cavity, Deppe and Deng [42–44] have expanded a radiation into planar-waves modes. They were using the complete and orthogonal set of base functions obtained with the aid of the source-free Maxwell equations.

A very interesting vectorial approach has been recently proposed by Noble *et al.* [45,46]. This model, principally analogous to the scalar effective index method, is called the weighted index method [47,48]. Its philosophy is different from all the above presented vectorial approaches. Instead of solving the exact vector wave equation with the aid of approximate base functions, Noble *et al.* [45] have replaced the exact equations with an approximate ones and have solved them exactly. Introducing the magnetic $\vec{A}$ and the electric $\vec{F}$ vector potentials, the vector wave equation for cylindrically symmetric structures will have the following scalar Helmholz form

$$\left\{\frac{\partial^2}{\partial r^2} + \frac{1}{r}\frac{\partial}{\partial r} + \frac{\partial^2}{\partial z^2} + \left[k_0^2 N_R^2 - \frac{k^2}{r^2}\right]\right\}\begin{Bmatrix} A_z(r,z) \\ F_z(r,z)\end{Bmatrix} = 0. \quad (44)$$

An arbitrary mode may be represented as a superposition of TE and TM modes [49], which are directly associated with the F_z and A_z potential components, respectively. Then both the electric and magnetic fields are given by [50]

$$\vec{E} = -\frac{i}{k_0 N_R^2}\nabla\times\nabla\times(A_z\cdot\vec{1}_z) - \nabla\times(F_z\cdot\vec{1}_z), \quad (45)$$

$$\vec{H} = \nabla\times(A_z\cdot\vec{1}_z) - \frac{i}{k_0\mu_0}\nabla\times\nabla\times(F_z\cdot\vec{1}_z), \quad (46)$$

which may be explicitly separated for all field components. In the above equations, $\vec{1}_z$ is the unit vector along the 0z coordinate.

Analogously to the effective index method, the weighted index method assumes separability of both A_z and F_z

$$A_z(r,z) = P(r)Q(z), \quad (47)$$

$$F_z(r,z) = R(r)S(z). \quad (48)$$

Substituting the above relations to Eq. (44), we reach two radial equations

$$\left[\frac{d^2}{dr^2} + \frac{1}{r}\frac{d}{dr} + (k_i^\alpha)^2 - \frac{k^2}{r^2}\right]\varsigma(r) = 0, \quad (49)$$

and two axial equations

$$\left[\frac{d^2}{dr^2} + (\beta_j^\alpha)^2\right]\xi(z) = 0, \quad (50)$$

where $\varsigma(r)$ = P(r) or R(r) and $\xi(z)$ = Q(z) or S(z), and α = TE or TM. A piecewise-constant refractive-index profile is assumed. The above radial and axial equations are coupled by the weighted axial and radial propagation constants k_i^α and β_j^α, where i and j indices are the radial and axial regions, respectively. The calculations should be repeated self-consistently for both the axial and the radial directions until propagation constants, in two consecutive calculation loops, remain practically unchanged.

7. Conclusions

Simulation of a VCSEL operation is often used to upgrade our knowledge of physical phenomena taking place inside its volume, i.e., to understand better physics of all interactions between various physical processes crucial for this operation. Very advanced computer devices, even supercomputers, are typically used in such simulations. The simulations require ample computer memories and high operation speeds to be implemented because an introduction of a whole complex network of many nonlinear and mutual interactions between various physical processes is critical for an exactness of physical modelling of this kind and none of them should be neglected.

VCSEL simulations are also (and maybe mostly) applied to an optimisation of a given VCSEL design or to its modification for a specified application. Applicability of any approach to this end is, however, immediately associated with a quality of the computer device used during this simulation. Therefore too sophisticated models, seemingly very exact and elaborate, may be completely useless if they need too long CPU time and/or too much memory of an available computer to be implemented. Hence both simplified and advanced optical VCSEL approaches should be available. And they both may be applied depending on an aim of a simulation and a quality of computer devices used. Besides simplified models are useful also during advanced modelling to verify its exactness. Nevertheless a rapid improvement in achievements of computer devices observed during last decades makes verification of usefulness of any approach still an open question. Too advanced and too involved models at present are steadily becoming more and more suitable even for standard-level computers. Therefore even the most sophisticated VCSEL models may have hope to become more popular in future.

Acknowledgements

This work was supported by the Polish State Committee for Scientific Research (KBN) under the grant # 8-T11B-018-12, by the Marie Curie-Skłodowska Foundation under the grant # MEN/NSF-98-336, and by the CFD Research Corporation, Huntsville, Alabama, USA.

References

1. W. Nakwaski, "Simulation of optical phenomena in vertical-cavity surface-emitting lasers. I. Fundamental principles", *Opto-Electr. Rev.* **8**, this issue.
2. Y.G. Zhao and J.G. McInerney, "Transverse-mode control of vertical-cavity surface-emitting lasers", *IEEE J. Quantum Electron.* **32**, 1950–1958 (1996).
3. V.A. Smagley, G.A. Smolyakov, P.G. Eliseev, M. Osiński, and A.J. Przekwas, "Current self-distribution effect in vertical-cavity surface-emitting semiconductor lasers", *Proc. SPIE* **3283**, 171–182 (1998).
4. W. Nakwaski, "Thermal aspects of efficient operation of vertical-cavity surface-emitting lasers", *Opt. Quantum Electron.* **2**, 335–352 (1996).
5. D. Gloge, "Weakly guiding fibers", *Appl. Opt.* **10**, 2252–2258 (1971).
6. E. Snitzer, "Cylindrical dielectric waveguide modes", *J. Opt. Soc. Am.* **51**, 491–498 (1961).
7. W. Nakwaski and R.P. Sarzała, "Higher-order transverse modes in vertical-cavity surface-emitting lasers", *Proc. SPIE* **3320**, 78–96 (1997).
8. D. Marcuse, *Light Transmission Optics*, Chapter 7.3, Van Nostrand, Reinholt Company, New York, 1972.
9. M. Abramowitz and I.A. Stegun, *Handbook of Mathematical Functions with Formulas, Graphs, and Mathematical Tables*, Dover Publications, New York, 1972.
10. Ref. 9, p. 785

11. W. Nakwaski and R.P. Sarzała, "Transverse modes in gain-guided vertical-cavity surface-emitting lasers", *Opt. Commun.* **148**, 63–69 (1998).
12. A.K. Jansen van Doorn, M.P. van Exter, and J.P. Woerdman, "Observation of wave front curvature inside a vertical-cavity surface-emitting laser", *Appl. Phys. Lett.* **66**, 3561–3563 (1995).
13. J.P. Zhang and K. Petermann, "Numerical analysis of transverse mode in gain-guided vertical cavity surface emitting lasers", *IEE Proc. Optoelectron.* **142**, 29–35 (1995).
14. J.P. Zhang, "Single mode power and modal behaviour in buried vertical-cavity surface-emitting lasers", *IEE Proc. Optoelectron.* **142**, 87–93 (1995).
15. J. Wilk, R.P. Sarzała and W. Nakwaski, "The spatial hole burning effect in gain-guided vertical-cavity surface-emitting lasers", *J. Phys. D: Appl. Phys.* **31**, L11–L15 (1998).
16. W. Nakwaski and M. Osiński, "Thermal properties of vertical-cavity surface-emitting semiconductor lasers", *Progress in Optics* **38**, 165–262 (1998).
17. G.C. Wilson, D.M. Kuchta, J.D. Walker, and J.S. Smith, "Spatial hole burning and self-focusing in vertical-cavity surface-emitting laser diodes", *Appl. Phys. Lett.* **64**, 542–544 (1994).
18. S.F. Yu and C.W. Lo, "Influence of transverse modes on the dynamic response of vertical cavity surface emitting lasers", *IEE Proc. Optoelectron.* **143**, 189–194 (1996).
19. S.F. Yu, W.N. Wong, P. Shum, and E.H. Li, "Theoretical analysis of modulation response and second-order harmonic distortion in vertical-cavity surface-emitting lasers", *IEEE J. Quantum Electron.* **32**, 2139–2147 (1996).
20. S.F. Yu, "Dynamic behavior of vertical-cavity surface--emitting lasers", *IEEE J. Quantum Electron.* **32**, 1168–1179 (1996).
21. S.F. Yu, "Modelling of diffused quantum wells vertical cavity surface emitting lasers", *Proc. SPIE* **3283**, 841–848 (1998).
22. W.M. Man and S.F. Yu, "Comprehensive modelling of diffused quantum-well vertical-cavity surface-emitting lasers", *IEEE J. Select. Topics Quantum Electron.* **4**, 715–722 (1998).
23. S.F. Yu, "An improved time-domain travelling-wave model for vertical-cavity surface-emitting lasers", *IEEE J. Quantum Electron.* **34**, 1938–1948 (1998).
24. G.R. Hadley, "Effective index model for vertical-cavity surface-emitting lasers", *Opt. Lett.* **20**, 1483–1485 (1995).
25. G.R. Hadley, K.L. Lear, M.E. Warren, K.D. Choquette, J.W. Scott, and S.W. Corzine, "Comprehensive numerical modelling of vertical-cavity surface-emitting lasers", *IEEE J. Quantum Electron.* **32**, 607–615 (1996).
26. H. Wenzel and H.J. Wünsche, "The effective frequency method in the analysis of vertical-cavity surface-emitting lasers", *IEEE J. Quantum Electron.* **33**, 1156–1162 (1997).
27. G.A. Smolyakov, V.A. Smagley, W. Nakwaski, P.G. Eliseev, and M. Osiński, "Design of InGaN/GaN/AlGaN VCSELs using the effective frequency method", *Proc. SPIE* **3625**, in print (1999).
28. M. Osiński, V.A. Smagley, G.A. Smolyakov, T. Svimonishvili, P.G. Eliseev, and G. Simonis, "Three-dimensional simulation of oxide-confined vertical-cavity surface-emitting semiconductor lasers", *Proc. SPIE* **3419**, 196–207 (1998).
29. M. Osiński, V.A. Smagley, T. Svimonishvili, G.A. Smolyakov, and P.G. Eliseev, "3D electro-thermal simulation of intracavity-contacted oxide-confined VCSELs operating at room-temperature and at 77 K", *Proc. SPIE* **3625**, in print (1999).
30. L.E. Thode, G. Csanak, L.L. So, J.T. Kwan, and M. Campbell, "Time-dependent numerical simulation of vertical cavity lasers", *Proc. SPIE* **2146**, 174–184 (1994).
31. C.Z. Ning and J.V. Moloney, "Plasma-heating induced intensity-dependent gain in semiconductor lasers", *Appl. Phys. Lett.* **66**, 559–561 (1995).
32. C.Z. Ning and J.V. Moloney, "Thermal effects on the threshold of vertical-cavity surface-emitting lasers: first- and second-order phase transitions", *Opt. Lett.* **20**, 1151–1153 (1995).
33. C.Z. Ning, R.A. Indik, and J.V. Moloney, "Self-consistent approach to thermal effects in vertical-cavity surface-emitting lasers", *J. Opt. Soc. Am.* B **12**, 1993–2004 (1995).
34. T. Rössler, R.A. Indik, G.K. Harkness, J.V. Moloney, and C.Z. Ning, "Modelling the interplay of thermal effects and transverse mode behavior in native-oxide-confined vertical-cavity surface-emitting lasers", *Phys. Rev.* A **58**, 3279–3292 (1998).
35. B. Demeulenaere, D. De Zutter, and R. Baets, "Rigorous electromagnetic study of diffraction loss in VCSEL mirrors", *IEE Proc. Optoelectron.* **143**, 221–227 (1996).
36. J.A. Kong, *Electromagnetic Wave Theory*, Wiley, 1986.
37. A.S. Omar and K.F. Schünemann, "The effect of complex modes in finline discontinuities", *IEEE Trans. Microwave Theory & Technique* **MTT-34**, 1508–1515 (1986).
38. A.S. Omar and K.F. Schünemann, "Complex and backward-wave modes in inhomogeneously and anisotropically filled waveguides", *IEEE Trans. Microwave Theory & Technique* **MTT-35**, 268–275 (1987).
39. D. Burak and R. Binder, "Cold-cavity vectorial eigenmodes of VCSEL's", *IEEE J. Quantum Electron.* **33**, 1205–1215 (1997).
40. D. Burak and R. Binder, "Theoretical study of electromagnetic eigenmodes of VCSEL's", *Proc. SPIE* **2994**, 159–167 (1997).
41. D. Burak and R. Binder R., "Role of carrier diffusion in semiconductor microdisk lasers", *Proc. SPIE* **2693**, 176–187 (1996).
42. D.G. Deppe and Q. Deng, "Self-consistent eigenmode analysis of the dielectrically apertured Fabry-Perot microcavity", *Appl. Phys. Lett.* **71**, 160–162 (1997).
43. Q. Deng and D.G. Deppe, "Self-consistent calculation of the lasing eigenmode of the dielectrically apertured Fabry--Perot microcavity with idealised or distributed Bragg reflectors", *IEEE J. Quantum Electron.* **33**, 2319–2326 (1997).
44. Q. Deng and D.G. Deppe, "Modelling the lasing mode in a 3-dimensionally confined Fabry-Perot microcavity", *Proc. SPIE* **2994**, 267–274 (1997).
45. M.J. Noble, J.P. Loehr, and J.A. Lott, "Calculation of microcavity VCSEL field modes using a doubly iterative weighted index method", *Proc. SPIE* **2994**, 259–266 (1997).
46. M.J. Noble, J.P. Loehr, and J.A. Lott, "Analysis of microcavity VCSEL lasing modes using a full-vector weighted index method", *IEEE J. Quantum Electron.* **34**, 1890–1903 (1998).

47. P. Kendall, M. Adams, S. Ritchie, and M. Robertson, "Theory for calculating approximate values for the propagation constants of an optical rib waveguide by weighting the refractive indices", *Proc. IEE* **134**, 699–702 (1987).
48. M. Robertson, P. Kendall, S. Ritchie, P. McIlroy, and M. Adams, "The weighted index method: A new technique for analysing planar optical waveguides", *J. Lightwave Technol.* **7**, 2105–2108 (1989).
49. R.F. Harrington, *Time-Harmonic Electromagnetic Fields*, pp. 186–189, Mc-Graw-Hill, New York, 1961.
50. J. Jackson, *Classical Electrodynamics*, Wiley, New York 1975.

